5-21-2019

Mechanism of Electrospray Supercharging for Unfolded Proteins: Solvent-Mediated Stabilization of Protonated Sites During Chain Ejection.

Insa Peters

Haidy Metwally

Lars Konermann

Mechanism of Electrospray Supercharging for Unfolded Proteins: Solvent-Mediated Stabilization of Protonated Sites During Chain Ejection

Insa Peters, Haidy Metwally, and Lars Konermann*

Department of Chemistry, The University of Western Ontario, London, Ontario, N6A 5B7, Canada.

* corresponding author: konerman@uwo.ca

Funding was provided by the Natural Sciences and Engineering Research Council of Canada (RGPIN-2018-04243).

ABSTRACT: Proteins that are unfolded in solution produce higher charge states during electrospray ionization (ESI) than their natively folded counterparts. Protein charge states can be further increased by the addition of supercharging agents (SCAs) such as sulfolane. The mechanism whereby these supercharged $[M + zH]^{z+}$ ions are formed under unfolded conditions remains unclear. Here we employed a combination of mass spectrometry (MS), ion mobility spectrometry (IMS), and molecular dynamics (MD) simulations for probing the ESI mechanism under denatured supercharging conditions. ESI of acid-unfolded apo-myoglobin (aMb) in the presence of sulfolane produced charge states around 27+, all the way to fully protonated (33+) aMb. MD simulations of aMb 27+ to 33+ in Rayleigh-charged water/sulfolane droplets culminated in electrostatically driven protein expulsion, consistent with the chain ejection model (CEM). The electrostatically stretched conformations predicted by these simulations were in agreement with IMS experiments. The CEM involves partitioning of mobile H^+ between the droplet and the departing protein. Our results imply that supercharging of unfolded proteins is caused by residual sulfolane that stabilizes protonated sites on the protruding chains, thereby promoting H^+ retention on the protein. The stabilization of charged sites is due to charge-dipole interactions mediated by the large dipole moment and the low volatility of sulfolane. Support for this mechanism comes from the experimental observation of sulfolane adducts on the most highly charged ions, a phenomenon previously noted by Venter (*J. Am. Soc. Mass Spectrom*. **2012**, *23*, 489-497). The "CEM supercharging model" proposed here for unfolded proteins is distinct from the charge trapping mechanism believed to be operative during native ESI supercharging.

Electrospray ionization (ESI) mass spectrometry (MS) and ion mobility spectrometry (IMS) are key techniques for the characterization of proteins.[1] Positive ESI produces gaseous $[M + zH]^{z+}$ ions. The behavior of these ions is governed by their charge state z; this includes their conformation,[2, 3] transmission,[4] fragmentation,[5, 6] reactivity,[7-9] and detection.[10, 11] Thus, being able to control protein charge states is important for many applications. Efforts to understand protein charging are closely intertwined with the question how analyte ions are formed from ESI nanodroplets.[12-22] Four modes of intact protein ESI (i-iv) can be distinguished:

(i) *Native ESI* aims to preserve solution structures and interactions in the gas phase. These studies use neutral aqueous solutions, and most proteins are folded as they enter the ESI source.[23-31] Despite some alternative proposals,[16-19] it is widely believed that native ESI proceeds via the charged residue model (CRM), where protein ions are released upon droplet evaporation to dryness.[12, 13, 25, 32] Emission of small charge carriers (H^+, Na^+, NH_4^+) via the ion evaporation mechanism (IEM) ensures that the shrinking droplets stay close to the Rayleigh limit.[21, 33-36] The resulting protein charge is determined by the number of charge carriers that bind to surface side chains as the last solvent layers evaporate.[12, 13, 25, 32, 37] Native ESI produces gaseous proteins with collision cross sections (Ω) that are consistent with solution-like conformations.[29, 30, 38, 39]

(ii) *Denaturing ESI* starts with unfolded proteins. Often these experiments use acidified aqueous solutions. Organic cosolvents may be present as well, but differential evaporation causes water enrichment during the droplet life cycle.[35, 40-42] Denaturing ESI generates protein ions that are more highly charged than in native ESI.[18, 43-48] These highly charged species likely form via the chain ejection model (CEM, Figure 1a).[49] According to the CEM, exposed hydrophobic residues cause the unfolded protein to migrate to the droplet surface. The chain then gets pushed out of the droplet via “tadpole” shaped intermediates. Chain ejection is driven by electrostatic repulsion

between the droplet and the protein. The formation of high charge states is attributed to H^+ that migrate onto the protein tail to minimize unfavorable Coulombic repulsion. Charge partitioning between droplet and protein is facilitated by the high H^+ mobility in water[50] and in gaseous proteins.[51-53] H^+ migration takes place until the protein detaches from the droplet.[25, 37, 49] The CEM bears analogies to the collision-induced dissociation (CID) of noncovalent protein complexes. Both processes involve H^+ migration with subsequent ejection of a highly charged[54-57] and highly extended[58, 59] chain. Similar extrusion scenarios also apply to synthetic polymers such as polyethylene glycol,[60] albeit without H^+ migration which is a key element of the protein CEM.[49]

Complementary to denaturing ESI, the use of supercharging agents (SCAs) allows the formation of highly charged protein ions.[8, 20, 61, 62] Typical SCAs such as sulfolane, $(CH_2)_4SO_2$, are added at low concentrations (~1%) that do not affect the protein structure in bulk solution.[63] Their low volatility makes them evaporate more slowly than water, such that late ESI droplets are SCA-enriched.[17, 63-65] SCAs possess a large dipole moment[65-67](4.7 D for sulfolane[68] vs. 1.85 D for water).[69] Their surface tension is between methanol and water,[65] and they exhibit a low Brønsted basicity.[66] The mechanisms whereby SCAs boost protein charge states are still under discussion.[17, 20, 40, 63, 64, 67, 70] Similar to the regular ESI experiments outlined above, two types of supercharging conditions can be distinguished.

(iii) *Native supercharging* employs SCAs in solutions where the protein remains folded, such that native-like conformations and interactions can be retained in the gas phase. Yet, the ions formed in this way have higher charge states than in regular native ESI.[64, 71] Work from our laboratory[70] suggested that native supercharging is a CRM process, with the caveat that SCAs form a surface layer on the droplet that interferes with ejection of charge carriers. This "charge trapping" causes a larger number of H^+, Na^+ or NH_4^+ to bind to the protein, thereby increasing the charge of the resulting ion. For details of this model and possible alternatives, see ref.[70]

(iv) *Denatured supercharging ESI* starts with proteins that are unfolded, typically in an acidified SCA-containing aqueous solution. The combination of solution-phase unfolding and SCA-mediated charge enhancement produces very highly protonated $[M + zH]^{z+}$ ions, up to the point where all basic sites (N-terminus (NT), Arg, Lys, His) carry a proton.[8, 65, 67] Even some less basic sites may participate.[72] The mechanism by which SCAs boost the ESI charge states of unfolded proteins is unknown. It has been proposed that denatured supercharging ESI proceeds via the CEM,[9, 73] but additional data are required to support this proposal. Venter[67] suggested that SCAs promote H^+ binding via charge-dipole contacts with the unfolded protein. However, it was not specified whether these putative contacts occur in solution, in the droplet, or at a later stage. Also, it is unclear if Venter's proposal[67] is compatible with the view that denatured supercharging ESI proceeds via the CEM.[9, 73]

Using ESI-IMS-MS and molecular dynamics (MD) simulations, the current work scrutinizes the mechanism of denatured supercharging ESI. MD simulations have addressed many ESI-related questions in recent years,[74-81] including protein ion formation under conditions (i),[32, 78, 79] (ii),[49] and (iii).[70] However, this approach has not yet been extended to denatured supercharging ESI (scenario iv). Here we close this gap. We focus on acid-unfolded myoglobin in the presence of sulfolane. Myoglobin has been used in numerous ESI investigations,[32, 44, 47, 49, 63, 64, 70] and sulfolane represents a prototypical SCA.[64, 65, 67] Our goals were twofold; first, we wanted to determine whether denatured supercharging ESI proceeds via the CEM.[73] Secondly, we wanted to elucidate why these conditions generate such highly charged ions, paying special attention to possible charge-dipole interactions.[67] Our results uncover that the two concepts go hand in hand. According to the *CEM supercharging model* proposed here, SCA-mediated charge solvation causes H^+ retention on acid-unfolded proteins during chain ejection.

Materials and Methods

Horse heart holo-myoglobin (hMb) was from Sigma, St. Louis, MO. Heme was removed by acidification in water/0.1 M HCl followed by washing in 10 kDa Millipore centrifuge filters. Resuspension yielded apo-myoglobin (aMb, pI ≈ 7.6). Native ESI samples contained 5 μM protein in 10 mM neutral aqueous ammonium acetate. Denaturing ESI was performed in aqueous formic acid (0.1%, pH 2.7). For supercharging 1% sulfolane was added to these acidified samples. Data were acquired on a Synapt G2 Si Q-TOF (Waters, Milford, MA). Solutions were infused at 5 μL min^{-1} using an ESI voltage of +2.8 kV. Most spectra were acquired at a cone voltage of 20 V, with source and desolvation temperatures of 80 °C and 250 °C, respectively. For travelling wave IMS and for retention of sulfolane adducts the cone voltage and temperatures were lowered (5 V, 25 °C, 40 °C). Low signal intensities under these conditions necessitated doubling of the aMb concentration. IMS arrival time distributions were converted to effective He Ω values.[49]

Gromacs 2016[82] with the Charmm36 force field[83] and TIP4P/2005 water[84] was used for MD simulations. Initial conformations were produced by exposing aMb^{22+} (1wla without heme) to 450 K for 1.5 ns in vacuum. The resulting linearized structures were converted to random coils in 0.1 ns runs at 350 K with zero charge. The aMb charge was then set to 27+, 30+, or 33+ by protonation of NT/Arg/Lys/His in different permutations. Acidic sites were neutral, consistent with the high proton affinity of $R\text{-}COO^-$.[85] Droplets with 5.5 nm radius were built around the protein (22,300 H_2O or 15,000 H_2O/1000 sulfolane). All runs started with a total charge of 47+, corresponding to the Rayleigh limit at 370 K.[49] This charge was attained by replacing random H_2O with Na^+. The droplets were equilibrated at 300 K for 8 ns. 75 ns ESI simulations were conducted at 370 K. All runs were repeated five times with different starting conformations and velocities. For Ω calculations using Collidoscope[86] residual solvent was removed, followed by 500 ns MD at

320 K. Coordinates from these runs were extracted in 100 ns intervals, and their Ω values were averaged.

Results and Discussion

ESI Mass Spectra: Implications for H^+ Migration. Figure 2 shows myoglobin spectra acquired under different conditions. Native ESI of hMb yielded heme-containing ions with 9+ as the dominant charge state (Figure 2a).[32, 44, 47, 63, 64] These ions represent CRM products.[12, 13, 25, 32]

Heme-free myoglobin (aMb) is conformationally heterogeneous in solution, consistent with its bimodal charge state distribution under native ESI conditions (Figure 2b).[44] Compact structures produced charge states around 9+, whereas unfolded aMb generated ions around 17+ and up to 28+.[44, 47] NH_4^+ is the main charge carrier under the conditions of Figure 2b,[13] likely producing a droplet pH of ~6.[87] At this pH the solution charge of aMb is about 10+ (Figure S1). Many of the aMb ions in Figure 2b have ESI charge states that greatly exceed this solution charge ($z_{solution} < z_{gas\ phase}$). The formation of these high ESI charge states from unfolded solution structures is attributed to the CEM, with H^+ migration from the droplet to the departing protein (Figure 1a).[25, 37, 49] Charge states around 9+ in Figure 2b likely represent CRM products.[12, 13, 25, 32, 81]

In 0.1% formic acid (pH 2.7) aMb is unfolded and completely protonated in solution ($z_{solution}$ = 33+, Figure S1).[44, 47] ESI of these proteins produced a charge state distribution with a maximum at 23+, implying that $z_{solution} > z_{gas\ phase}$ (Figure 2c). Thus, the CEM under these conditions must involve *reverse* H^+ migration, where the departing protein leaves some of its charge behind on the droplet (Figure 1b).[25, 37, 49] In other words, the direction of H^+ migration during the CEM depends on the difference between $z_{solution}$ and $z_{gas\ phase}$. Previous CEM discussions largely focused on the scenario of Figure 1a.[25, 37, 49] The reverse H^+ migration postulated in Figure 1b represents an extension of the CEM to cases where $z_{solution} > z_{gas\ phase}$.

Denatured supercharging ESI was implemented by adding 1% sulfolane to the pH 2.7 solutions. The resulting ions were very highly charged, with 27+ as the most intense peak. The highest observable charge state was 33+, very close to the most highly supercharged aMb ions (34+) previously reported in the literature.[8, 88] (Figure 2d). The objective of the subsequent discussion is to decipher the mechanism of ion formation under the conditions of Figure 2d.

Sulfolane Adducts. The spectra in Figure 2a-d were acquired using standard settings. With reduced source activation the highest charge states (29+ to 33+) generated by denatured supercharging ESI retained up to four sulfolane molecules, while these adducts were less abundant or undetectable for lower charge states (Figure 2e-i, Figure S2). The use of harsher conditions resulted in adduct removal for all charge states (Figure S3). Because SCAs have low volatility,[17, 63-65] sulfolane adduction may not seem surprising.[13, 26] However, nonspecific adducts typically affect low charge states to a greater extent than highly charged ions, reflecting the fact that in-source activation is proportional to z.[26, 64, 89] Figure 2e-i shows the opposite trend, i.e., sulfolane adducts are seen only for the most highly charged ions. This observation suggests that *sulfolane binding to unfolded aMb may be directly involved in the formation of high charge states*. Such a scenario is consistent with the work of Venter, where similar adduction trends were reported for supercharged cytochrome *c*.[67] It is noted, however, that sulfolane adduction in our aMb experiments is much more prevalent than that reported by Venter.[67] We will return to the mechanistic implications of these adducts after discussing some MD results.

Unfolded aMb in Water/Sulfolane Follows the CEM. MD simulations on CEM phenomena are challenging because standard force fields employ fixed charges that cannot account for H^+ migration.[82] Our previous CEM work (without SCAs)[49] sidestepped this issue by focusing on a pH

regime where $z_{solution} = z_{gas\ phase}$, such that H^+ migration could be neglected. Here we pursued a similar strategy. Acid-unfolded aMb at pH 2.7 has a 33+ solution charge (Figure S1), matching the charge of gaseous aMb^{33+}. Unfortunately, aMb^{33+} has very low abundance in the experimental spectra (Figure 2c/d). For probing the behavior of more "typical" ions, it would thus be desirable to examine aMb in somewhat lower charge sates. We decided to model aMb^{27+} and aMb^{30+}, in addition to aMb^{33+}. The former two are still in a regime where $z_{solution} \approx z_{gas\ phase}$, such that fixed charge MD runs should capture their qualitative behavior. We will start by discussing aMb^{27+} which has the highest intensity in denatured supercharging ESI (Figure 2d) and is abundant even without supercharging (Figure 2c).

Figure 3a illustrates CEM behavior for unfolded aMb^{27+} in water without sulfolane.[49] Within 6.5 ns the protein migrated to the surface. At t = 7.3 ns the chain erupted, forming a tail that grew in length as the rest of the protein was ejected. After 25.8 ns, aMb detached from the droplet. This overall scenario was highly reproducible, but the exact separation time point varied from run to run (Figure S4a).[49] The CEM was accompanied by occasional IEM ejection of Na^+, and gradual solvent evaporation (Figure 4a/b, Figure S4a). However, droplet shrinkage was much less prevalent than in CRM runs on folded proteins where solvent evaporates to dryness.[12, 13, 25, 32]

Water/sulfolane droplets containing unfolded aMb^{27+} also followed the CEM, with gradual protein ejection followed by separation from the droplet (Figure 3b). This CEM behavior was confirmed in multiple runs (Figure S4b). The water/sulfolane droplets exhibited moderate SCA surface enrichment (Figure 3b top, Figure S5). CEM behavior was also seen for aMb^{30+} and aMb^{33+} in water/sulfolane. These more highly charged ions tended to separate from the droplet later, after more water evaporation had taken place. Evaporation statistics for these 30+/33+ runs are compiled in Figure S4c/d, and representative MD snapshots are shown in Figures S6, S7.

The CEM events for most $aMb^{27+/30+/33+}$ sulfolane/water runs were similar to those in Figure 3b, but there was some variability in the morphology of the intermediate stages. In one case the protruding chain initially remained associated with a small droplet, prior to forming a CEM "tadpole" (Figure S8a). In another run, the protein emerged as a loop that subsequently opened up (Figure S8b). In the latter instance protein and droplet did not separate; instead, the droplet dried out while remaining attached to the protein tail. Such a CEM/CRM hybrid scenario[37] was observed only once, while all other (14/15) water/sulfolane runs showed regular CEM behavior.

For both water and water/sulfolane, the protein retained a significant number of solvent molecules after separating from the droplet. Water continued to evaporate rapidly from the protein. Sulfolane loss occurred at a much slower rate, consistent with its low vapor pressure (Figure 4a/c, Figure S4)[17, 63-65] and with the experimentally observed sulfolane adducts (Figure 2, Figure S4).

Our simulations predicted that CEM-generated aMb ions adopt electrostatically stretched conformations. This prediction was confirmed in IMS experiments that yielded Ω values around 4000 Å for $aMb^{27+/30+/33+}$. Ω values of the near-linear gaseous MD ions fell within the range of the experimental Ω distributions (Figure S9). The agreement between MD results and IMS experiments bolsters the validity of the simulation strategy used. In summary, our computational and experimental data support the proposal[9, 73] that denatured supercharging ESI generates protein ions via the CEM.

CEM Supercharging is Mediated by Solvation. The charge of CEM-generated protein ions is determined by the number of H^+ residing on the chain as it separates from the droplet (Figure 1a/b).[25, 37, 49] When considering only droplet and protein, it is difficult to envision why sulfolane would cause the presence of additional H^+. The missing piece of the puzzle is *charge solvation*, which plays a central role in governing H^+ behavior.[22, 90, 91] We will focus on aMb^{27+} which is

abundant in experiments conducted with and without sulfolane (Figure 2c/d). Figure 5 shows MD structures of aMb^{27+} that is about to separate from a water droplet and a water/sulfolane droplet. In both cases, the protein retains numerous solvent molecules (Figure 5a-c).

Electrostatic analyses were performed to scrutinize the solvation of NT^+, Arg^+, Lys^+, and His^+ immediately (~100 ps) after separation from the droplets. Interaction energies were calculated as $E_{ij} = (4\pi\varepsilon_0)^{-1}\, q_i\, q_j\, /\, r_{ij}$. Charges q_i and q_j were taken from the force field, and distances r_{ij} were determined from MD atomic coordinates. Judicious summation of these E_{ij} terms yielded the energies $E_{protein}$ and $E_{solvent}$. The former reflects the interactions of all charged sites with the rest of the protein. The latter reports on interactions of all charged sites with residual solvent. The overall energy of the charged sites is $E_{tot} = E_{protein} + E_{solvent}$. Both water and water/sulfolane yielded similar $E_{protein}$ values around +5000 kJ mol^{-1} (Figure 5d). The positive sign of $E_{protein}$ reflects the prevalence of repulsive (+) (+) contacts within the nascent protein ions. In contrast, strongly negative $E_{solvent}$ values arose from attractive charge-dipole interactions between NT^+/Arg^+/Lys^+/His^+ and solvent molecules. These favorable (+) (– +) contributions were more prevalent in the presence of sulfolane, because the sulfolane dipole moment is 2.5 times greater than that of water.[68, 69] As a result of these favorable solvation effects, E_{tot} was ~4000 kJ mol^{-1} lower in the presence of sulfolane (Figure 5d).

What are the implications of this lower E_{tot} in the presence of sulfolane? Under acidic conditions the CEM involves H^+ migration from the protein to the droplet (Figure 1b). Solvation by sulfolane will stabilize H^+ that reside on NT/Arg/Lys/His by lowering the electrostatic energy, thereby suppressing H^+ migration to the droplet. In other words, solvation by sulfolane increases the capacity of these basic sites to accommodate H^+ (Figure 1c).

Can electrostatic analyses predict the extent of supercharging? Basic protein sites have proton affinities[85] of ~1000 kJ mol^{-1}. Thus, the value of $\Delta E_{tot} \approx 4000$ kJ mol^{-1} in Figure 5d is

roughly equivalent to four protonation events ($\Delta z \approx 4$). This estimate matches the experimental charge state maxima of 23+ in water and 27+ in water/sulfolane (Figure 2c/d).

Not all nascent CEM ions carry the same number of solvent molecules. Solvation differences will arise from heterogeneities in droplet composition and/or size.[13] Our CEM supercharging model (Figure 1c) envisions that those chains that bind the most sulfolane molecules will form the highest charge states. This prediction is supported by our experiments, which showed that the highest charge states are most heavily sulfolane-adducted (Figures 2e-i). These adducts are remnants of the solvation shell that stabilized protein-bound H^+ during ejection (Figure 5b). The mechanism of Figure 1c extends the work of Venter[67] who first proposed the involvement of protein/SCA contacts in denatured supercharging ESI.

A Toy Model for CEM Supercharging. We designed a simple model to qualitatively illustrate the CEM supercharging mechanism, including H^+ migration processes that were not captured by our MD simulations. Figure 6 depicts a minimalist ESI droplet that is about to separate from a protein with three basic residues. The overall 10+ charge is treated as continuum. The droplet and the three residues are modeled as spherical conductors. Charge partitioning among the four spheres is governed by the tendency to minimize electrostatic energy. The protein charge $q_{protein} = q_1 + q_2 + q_3$ is modulated by solvent dipoles that interact with the protruding chain. A dipole moment of 1.85 D (water)[69] resulted in $q_{protein} = +1.29$. Upon raising the dipole moment to 4.7 D (sulfolane)[68] $q_{protein}$ increased to +1.61. This 25% increase represents supercharging under denaturing ESI conditions. The model of Figure 6 lacks atomistic details but it nonetheless captures the essential point of CEM supercharging, i.e., binding of strong dipoles (sulfolane or other SCAs) to the protruding chain increases $q_{protein}$.

Conclusions

The current work has attained two goals. (1) Our MD data confirmed that denatured supercharging ESI proceeds via the CEM.[9, 73] Because aMb is a commonly used model protein[32, 44, 47, 49, 63, 64, 70] and sulfolane represents a prototypical SCA,[64, 65, 67] the insights obtained here can likely be generalized. (2) We uncovered the mechanism whereby SCAs boost protein charge in denatured supercharging ESI, building on the work of Venter.[67] CEM supercharging is caused by residual solvent molecules that stabilize protonated basic sites on the protruding protein via charge-dipole interactions (Figure 1c). In the absence of these interactions, electrostatically driven H^+ migration would cause the acid-unfolded chain to lose a significant fraction of its charge to the droplet (Figure 1b). The ability of SCAs to exert this effect is linked to their low volatility[17, 63-65] which causes them to remain associated with the protruding chain. In addition, the mechanism relies on the high dipole moment of SCAs,[65, 66] which allows them to engage in much stronger charge-dipole contacts than water. This last point fits with the experimental observation that supercharging increases with increasing SCA dipole moment,[67] although other physicochemical parameters can play a role as well.[66, 92] Also, it is possible that gas phase H^+ transfer might alter the charge states of protein ions after their release from the droplet.[9, 93]

Finally, the CEM supercharging model proposed here for *acid-unfolded* proteins is fundamentally different from the *native* supercharging mechanism uncovered earlier.[70] Native supercharging involves folded proteins that are released upon droplet evaporation to dryness (CRM). Native supercharging has been attributed to charge trapping, i.e., the formation of a SCA layer around the aqueous/protein droplet core. This SCA layer interferes with IEM ejection of charge carriers from the droplet, thereby promoting charge carrier binding to the folded protein.[70] In contrast, under denaturing conditions SCA surface accumulation is not very prevalent (Figure S5), resulting in indistinguishable Na^+ IEM rates with and without sulfolane (Figure 4b/d). We

started the current work with the expectation that an SCA layer on the droplet surface would also be responsible for supercharging of acid-unfolded proteins. Instead, our MD simulations uncovered a very different supercharging mechanism (Figure 1c).[9, 17, 63-67, 73] It is hoped that future experimental and computational studies will continue to reveal fundamental aspects related to the formation of gaseous biomolecular ions during ESI.

References

(1) Fenn, J. B. *Angew. Chem. Int. Ed.* **2003**, *42*, 3871-3894.
(2) Laszlo, K. J.; Munger, E. B.; Bush, M. F. *J. Am. Chem. Soc.* **2016**, *138*, 9581-9588.
(3) Shelimov, K. B.; Clemmer, D. E.; Hudgins, R. R.; Jarrold, M. F. *J. Am. Chem. Soc.* **1997**, *119*, 2240-2248.
(4) Covey, T. R.; Thomson, B. A.; Schneider, B. B. *Mass Spectrom. Rev.* **2009**, *28*, 870-897.
(5) Yin, S.; Loo, J. A. *Int. J. Mass Spectrom.* **2011**, *300*, 118-122.
(6) Compton, P. D.; Zamdborg, L.; Thomas, P. M.; Kelleher, N. L. *Anal. Chem.* **2011**, *83*, 6868-6874.
(7) McLuckey, S. A.; Van Berkel, G. J.; Glish, G. L. *J. Am. Chem. Soc.* **1990**, *112*, 5668-5670.
(8) Ke, M. F.; Zhang, H.; Ding, J. H.; Xiong, X. C.; Li, F. L.; Chingin, K.; Kou, W.; Liu, A. Y.; Zhu, T. G.; Fang, X.; Chen, H. W. *Anal. Chem.* **2019**, *91*, 3215-3220.
(9) Zenaidee, M. A.; Leeming, M. G.; Zhang, F. T.; Funston, T. T.; Donald, W. A. *Angew. Chem.-Int. Edit.* **2017**, *56*, 8522-8526.
(10) Marshall, A. G.; Hendrickson, C. L.; Jackson, G. S. *Mass Spectrom. Rev.* **1998**, *17*, 1-35.
(11) Zubarev, A. R.; Makarov, A. *Anal. Chem.* **2013**, *85*, 5288-5296.
(12) de la Mora, F. J. *Anal. Chim. Acta* **2000**, *406*, 93-104.
(13) Kebarle, P.; Verkerk, U. H. *Mass Spectrom. Rev.* **2009**, *28*, 898-917.
(14) Cole, R. B. *J. Mass. Spectrom.* **2000**, *35*, 763-772.
(15) Cech, N. B.; Enke, C. G. *Mass Spectrom. Rev.* **2001**, *20*, 362-387.
(16) Nguyen, S.; Fenn, J. B. *Proc. Natl. Acad. Sci. U.S.A.* **2007**, *104*, 1111-1117.
(17) Ogorzalek Loo, R. R.; Lakshmanan, R.; Loo, J. A. *J. Am. Soc. Mass Spectrom.* **2014**, *25*, 1675-1693.
(18) Li, J.; Santambrogio, C.; Brocca, S.; Rossetti, G.; Carloni, P.; Grandori, R. *Mass Spectrom. Rev.* **2016**, *35*, 111-122.
(19) Siu, K. W. M.; Guevremont, R.; Le Blanc, J. C. Y.; O'Brien, R. T.; Berman, S. S. *Org. Mass Spectrom.* **1993**, *28*, 579-584.
(20) Iavarone, A. T.; Williams, E. R. *J. Am. Chem. Soc.* **2003**, *125*, 2319-2327.
(21) Hogan, C. J.; Carroll, J. A.; Rohrs, H. W.; Biswas, P.; Gross, M. L. *Anal. Chem.* **2009**, *81*, 369-377.
(22) Hamdy, O. M.; Julian, R. R. *J. Am. Soc. Mass Spectrom.* **2012**, *23*, 1-6.
(23) Nguyen, G. T. H.; Tran, T. N.; Podgorski, M. N.; Bell, S. G.; Supuran, C. T.; Donald, W. A. *ACS Centr. Sci.* **2019**, *5*, 308–318.
(24) Leney, A. C.; Heck, A. J. R. *J. Am. Soc. Mass Spectrom.* **2017**, *28*, 5-13.
(25) Mehmood, S.; Allison, T. M.; Robinson, C. V. *Annu. Rev. Phys. Chem.* **2015**, *66*, 453-474.
(26) Kitova, E. N.; El-Hawiet, A.; Schnier, P. D.; Klassen, J. S. *J. Am. Soc. Mass Spectrom.* **2012**, *23*, 431-441.
(27) Gavriilidou, A. F. M.; Holding, F. P.; Mayer, D.; Coyle, J. E.; Veprintse, D. B.; Zenobi, R. *Biochemistry* **2018**, *57*, 1685-1689.
(28) Dyachenko, A.; Gruber, R.; Shimon, L.; Horovitz, A.; Sharon, M. *Proc. Natl. Acad. Sci. U.S.A.* **2013**, *110*, 7235-7239.
(29) Wyttenbach, T.; Bowers, M. T. *J. Phys. Chem. B* **2011**, *115*, 12266-12275.
(30) Bush, M. F.; Hall, Z.; Giles, K.; Hoyes, J.; Robinson, C. V.; Ruotolo, B. T. *Anal. Chem.* **2010**, *82*, 9667-9565.
(31) Hendricks, N. G.; Julian, R. R. *Analyst* **2016**, *141*, 4534-4540.

(32) McAllister, R. G.; Metwally, H.; Sun, Y.; Konermann, L. *J. Am. Chem. Soc.* **2015**, *137*, 12667-12676.
(33) Iribarne, J. V.; Thomson, B. A. *J. Chem. Phys.* **1976**, *64*, 2287-2294.
(34) Consta, S. *J. Mol. Struct. (Theochem)* **2002**, *591*, 131-140.
(35) Grimm, R. L.; Beauchamp, J. L. *J. Phys. Chem. A* **2010**, *114*, 1411-1419.
(36) Allen, S. J.; Schwartz, A. M.; Bush, M. F. *Anal. Chem.* **2013**, *85*, 12055−12061.
(37) Beveridge, R.; Phillips, A. S.; Denbigh, L.; Saleem, H. M.; MacPhee, C. E.; Barran, P. E. *Proteomics* **2015**, *15*, 2872-2883.
(38) Jurneczko, E.; Barran, P. E. *Analyst* **2011**, *136*, 20-28.
(39) Hopper, J. T. S.; Oldham, N. J. *J. Am. Soc. Mass Spectrom.* **2009**, *20*, 1851-1858.
(40) Samalikova, M.; Grandori, R. *J. Am. Chem. Soc.* **2003**, *125*, 13352-13353.
(41) Wang, R.; Zenobi, R. *J. Am. Soc. Mass Spectrom.* **2010**, *21*, 378-385.
(42) Zhou, S.; Cook, K. D. *Anal. Chem.* **2000**, *72*, 963-969.
(43) Chowdhury, S. K.; Katta, V.; Chait, B. T. *J. Am. Chem. Soc.* **1990**, *112*, 9012-9013.
(44) Dobo, A.; Kaltashov, I. A. *Anal. Chem.* **2001**, *73*, 4763-4773.
(45) Borysic, A. J. H.; Radford, S. E.; Ashcroft, A. E. *J. Biol. Chem.* **2004**, *279*, 27069-27077.
(46) Rob, T.; Wilson, D. J. *J. Am. Soc. Mass Spectrom.* **2009**, *20*, 124-130.
(47) Fisher, C. M.; Kharlamova, A.; McLuckey, S. A. *Anal. Chem.* **2014**, *86*, 4581-4588.
(48) Loo, J. A.; Edmonds, C. G.; Udseh, H. R.; Smith, R. D. *Anal. Chem.* **1990**, *62*, 693-698.
(49) Metwally, H.; Duez, Q.; Konermann, L. *Anal. Chem.* **2018**, *90*, 10069-10077.
(50) Chen, M.; Zheng, L. X.; Santra, B.; Ko, H. Y.; DiStasio, R. A.; Klein, M. L.; Car, R.; Wu, X. F. *Nat. Chem.* **2018**, *10*, 413-419.
(51) Boyd, R. K.; Somogyi, Á. *J. Am. Soc. Mass Spectrom.* **2010**, *21*, 1275-1278.
(52) Dongré, A. R.; Jones, J. L.; Somogyi, Á.; Wysocki, V. H. *J. Am. Chem. Soc.* **1996**, *118*, 8365-8374.
(53) Li, J. Y.; Lyu, W. P.; Rossetti, G.; Konijnenberg, A.; Natalello, A.; Ippoliti, E.; Orozco, M.; Sobott, F.; Grandori, R.; Carloni, P. *J. Phys. Chem. Lett.* **2017**, *8*, 1105-1112.
(54) Schwartz, B. L.; Bruce, J. E.; Anderson, G. A.; Hofstadler, S. A.; Rockwood, A. L.; Smith, R. D.; Chilkoti, A.; Stayton, P. S. *J. Am. Soc. Mass Spectrom.* **1995**, *6*, 459-465.
(55) Felitsyn, N.; Kitova, E. N.; Klassen, J. S. *Anal. Chem.* **2001**, *73*, 4647-4661.
(56) Benesch, J. L. P. *J. Am. Soc. Mass Spectrom.* **2009**, *20*, 341-348.
(57) Fegan, S. K.; Thachuk, M. *J. Chem. Theory Comput.* **2013**, *9*, 2531-2539.
(58) Shelimov, K. B.; Jarrold, M. F. *J. Am. Chem. Soc.* **1997**, *119*, 2987-2994.
(59) Koeniger, S. L.; Clemmer, D. E. *J. Am. Soc. Mass Spectrom.* **2007**, *18*, 322-331.
(60) Consta, S.; Chung, J. K. *J. Phys. Chem. B* **2011**, *115*, 10447-10455.
(61) Lomeli, S. H.; Yin, S.; Loo, R. R. O.; Loo, J. A. *J. Am. Soc. Mass Spectrom.* **2009**, *20*, 593-596.
(62) Keener, J. E.; Zambrano, D. E.; Zhang, G. Z.; Zak, C. K.; Reid, D. J.; Deodhar, B. S.; Pemberton, J. E.; Prell, J. S.; Marty, M. T. *J. Am. Chem. Soc.* **2019**, *141*, 1054-1061.
(63) Sterling, H. J.; Daly, M. P.; Feld, G. K.; Thoren, K. L.; Kintzer, A. F.; Krantz, B. A.; Williams, E. R. *J. Am. Soc. Mass Spectrom.* **2010**, *21*, 1762-1774.
(64) Lomeli, S. H.; Peng, I. X.; Yin, S.; Ogorzalek Loo, R. R.; Loo, J. A. *J. Am. Soc. Mass Spectrom.* **2010**, *21*, 127-131.
(65) Teo, C. A.; Donald, W. A. *Anal. Chem.* **2014**, *86*, 4455-4462.
(66) Nshanian, M.; Lakshmanan, R.; Chen, H.; Ogorzalek Loo, R. R.; Loo, J. A. *Int. J. Mass Spectrom.* **2018**, *427*, 157–164.
(67) Douglass, K. A.; Venter, A. R. *J. Am. Soc. Mass Spectrom.* **2012**, *23*, 489-497.

(68) Tilstam, U. *Org. Process Res. Dev.* **2012**, *16*, 1273-1278.
(69) Liu, H. C.; Wang, Y. M.; Bowman, J. M. *J. Phys. Chem. B* **2016**, *120*, 1735-1742.
(70) Metwally, H.; Konermann, L. *Anal. Chem.* **2018**, *90*, 4126-4134.
(71) Hall, Z.; Politis, A.; Bush, M. F.; Smith, L. J.; Robinson, C. V. *J. Am. Chem. Soc.* **2012**, *134*, 3429-3438.
(72) Schnier, P. D.; Gross, D. S.; Williams, E. R. *J. Am. Soc. Mass Spectrom.* **1995**, *6*, 1086-1097.
(73) Donor, M. T.; Ewing, S. A.; Zenaidee, M. A.; Donald, W. A.; Prell, J. S. *Anal. Chem.* **2017**, *89*, 5107-5114.
(74) Znamenskiy, V.; Marginean, I.; Vertes, A. *J. Phys. Chem. A* **2003**, *107*, 7406-7412.
(75) Caleman, C.; van der Spoel, D. *Phys. Chem. Chem. Phys.* **2007**, *9*, 5105-5111.
(76) Higashi, H.; Tokumi, T.; Hogan, C. J.; Suda, H.; Seto, T.; Otani, Y. *Phys. Chem. Chem. Phys.* **2015**, *17*, 15746-15755.
(77) Porrini, M.; Rosu, F.; Rabin, C.; Darre, L.; Gomez, H.; Orozco, M.; Gabelica, V. *ACS Central Sci.* **2017**, *3*, 454–461.
(78) Kim, D.; Wagner, N.; Wooding, K.; Clemmer, D. E.; Russell, D. H. *J. Am. Chem. Soc.* **2017**, *139*, 2981-2988.
(79) Kondalaji, S. G.; Khakinejad, M.; Valentine, S. J. *J. Am. Soc. Mass Spectrom.* **2018**, *29*, 1665-1677.
(80) Consta, S.; Oh, M. I.; Kwan, V.; Malevanets, A. *J. Am. Soc. Mass Spectrom.* **2018**, *29*, 2287-2296.
(81) Beveridge, R.; Migas, L. G.; Das, R. K.; Pappu, R. V.; Kriwacki, R. W.; Barran, P. E. *J. Am. Chem. Soc.* **2019**, *141*, 4908-4918.
(82) Abraham, M. J.; Murtola, T.; Schulz, R.; Páll, S.; Smith, J. C.; Hess, B.; Lindahl, E. *SoftwareX* **2015**, *1–2*, 19-25.
(83) Huang, J.; MacKerell, A. D. *J. Comput. Chem.* **2013**, *34*, 2135-2145.
(84) Abascal, J. L. F.; Vega, C. *J. Chem. Phys.* **2005**, *123*, 234505.
(85) Moser, A.; Range, K.; York, D. M. *J. Phys. Chem. B* **2010**, *114*, 13911-13921.
(86) Ewing, S. A.; Donor, M. T.; Wilson, J. W.; Prell, J. S. *J. Am. Soc. Mass Spectrom.* **2017**, *28*, 587-596.
(87) Konermann, L. *J. Am. Soc. Mass Spectrom.* **2017**, *28*, 1827-1835.
(88) Wang, H.; Yong, G.; Brown, S. L.; Lee, H. E.; Zenaidee, M. A.; Supuran, C. T.; Donald, W. A. *Anal. Chim. Acta* **2018**, *1003*, 1-9.
(89) Thomson, B. A. *J. Am. Soc. Mass Spectrom.* **1997**, *8*, 1053-1058.
(90) Schnier, P. D.; Gross, D. S.; Williams, E. R. *J. Am. Chem. Soc.* **1995**, *117*, 6747-6757.
(91) Warnke, S.; von Helden, G.; Pagel, K. *J. Am. Chem. Soc.* **2013**, *135*, 1177-1180.
(92) Foley, E. D. B.; Zenaidee, M. A.; Tabor, R. F.; Ho, J.; Beves, J. E.; Donald , W. A. *Anal. Chim. Acta X* **2019**, *1*, 100004.
(93) Sterling, H. J.; Prell, J. S.; Cassou, C. A.; Williams, E. R. *J. Am. Soc. Mass Spectrom.* **2011**, *22*, 1178-1186.

Figure Captions

Figure 1. Three CEM scenarios, all starting with an unfolded protein in a 47+ droplet. The protein charge is denoted as z. (a) pH < pI, $z_{solution}$ = 10+. H^+ migration from the droplet to the departing chain increases the protein charge to $z_{gas\ phase}$ = 23+. (b) pH << pI, $z_{solution}$ = 33+. Reverse H^+ migration lowers the protein charge to $z_{gas\ phase}$ = 23+. (c) CEM supercharging. The conditions are similar to scenario (b), except for the presence of sulfolane. Sulfolane forms charge-dipole contacts that stabilize H^+ on the protruding chain, suppressing reverse H^+ migration and causing supercharging ($z_{gas\ phase}$ = 27+). Charge states in these cartoons resemble those of our experiments and MD simulations.

Figure 2. Myoglobin mass spectra. (a) hMb, native ESI, 10 mM aqueous ammonium acetate, neutral pH. (b) aMb, native ESI. (c) aMb, denaturing ESI, 0.1% aqueous formic acid. (d) aMb, denatured supercharging ESI, 0.1% aqueous formic acid with 1% sulfolane. (e) to (i): aMb charge states 33+ to 25+ produced by denatured supercharging ESI with gentle source settings. Up to four sulfolane adducts are discernible for the highest charge states (ΔM = 120 Da). Lower charge states carry no sulfolane adducts (see also Figure S2).

Figure 3. MD snapshots, illustrating CEM behavior for acid-unfolded aMb^{27+}. (a) Water droplet; (b) water/sulfolane droplet. The protein is shown in magenta, Na^+ are depicted in dark blue. Positively charged sites on the protein are shown as cyan spheres. For sulfolane, oxygen is red, sulfur is yellow, and C_4H_8 is green. The top panel in (b) shows a close-up of the droplet surface. Movies of these trajectories are included in the Supporting Information.

Figure 4. Number of solvent molecules and Na^+ in the system during the CEM for aMb^{27+}. (a) Solvent evaporation for a water droplet. (b) IEM ejection of Na^+ from water droplets prior to protein detachment, averaged over five runs. (c) Solvent evaporation for a water/sulfolane droplet. Arrows in (a), (c) indicate protein separation from the droplet. (d) IEM ejection of Na^+ for water/sulfolane droplets. A typical IEM event is illustrated in Figure S6.

Figure 5. MD snapshots, depicting aMb^{27+} that is about to separate from the ESI droplet. (a) Water droplet at 25.5 ns. (b) Water/sulfolane droplet at 14.8 ns. Close-ups highlight charged residues K77-K102 and their solvation by residual (a) water and (b) water/sulfolane. Coloring is as in Figure 3. Panels (c), (d) are for aMb^{27+} immediately (~100 ps) after separation from the droplets, averaged over five runs for each condition. (c) Number of solvent molecules attached to the protein. (d) Interaction energy of all $NT^+/Arg^+/Lys^+/His^+$ sites with the rest of the protein ($E_{protein}$) and with the residual solvent shell ($E_{solvent}$). E_{total} is the sum of these two terms.

Figure 6. Electrostatic toy model of CEM supercharging. A protein (magenta) is about to separate from an ESI droplet. Charge can partition among the droplet and three basic residues, all of which are modeled as spherical conductors. Charge accumulation on the protein is modulated by three dipolar solvent molecules. The protein charge ($q_{protein} = q_1 + q_2 + q_3$, magenta) is significantly higher when these dipoles are modeled as sulfolane (4.7 D) rather than water (1.85 D). For additional details, see Figure S10.

Figure 1

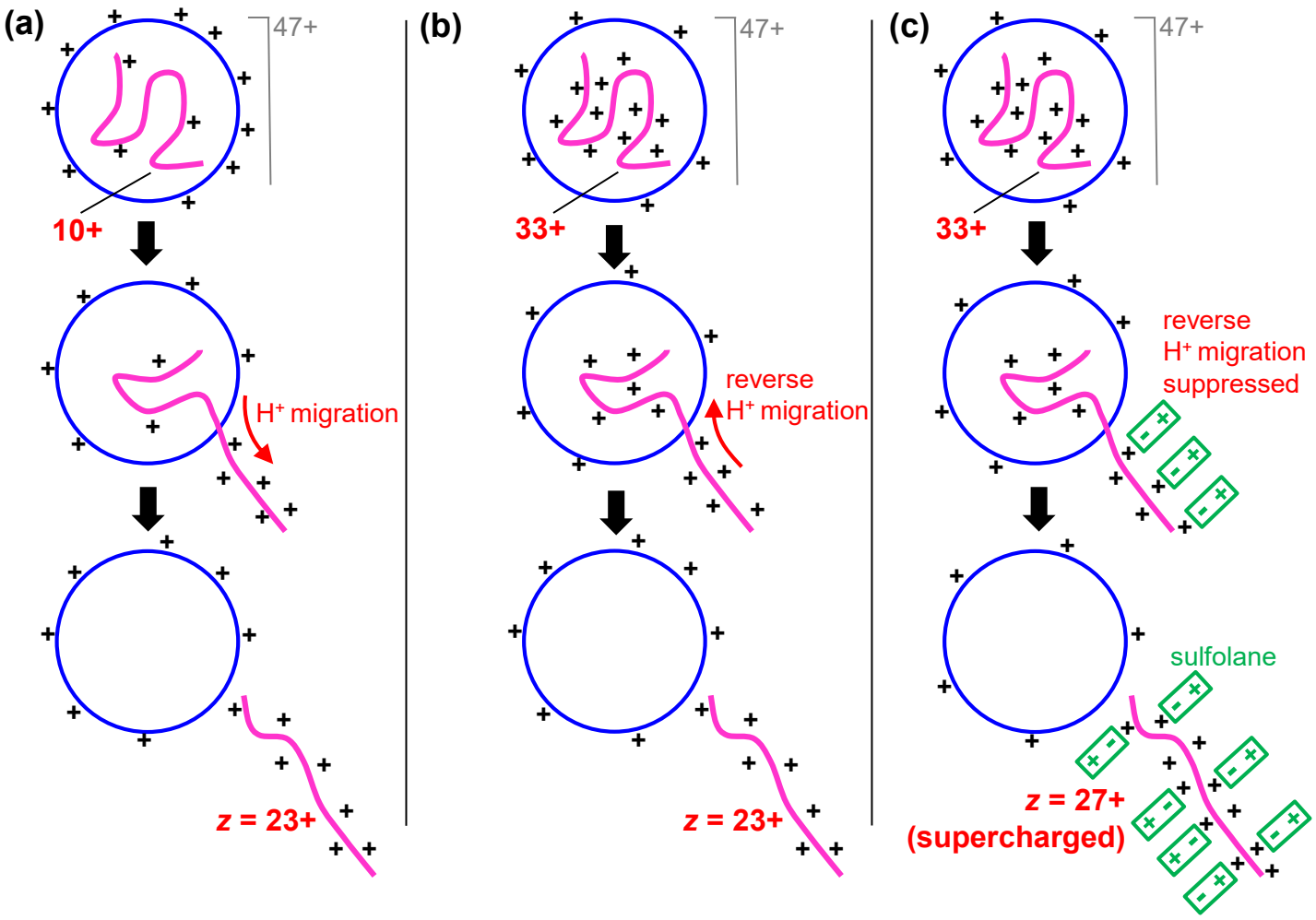
(a)
47+
10+
H⁺ migration
z = 23+
(b)
47+
33+
reverse
H⁺ migration
z = 23+
(c)
47+
33+
reverse
H⁺ migration
suppressed
sulfolane
z = 27+
(supercharged)

Figure 2

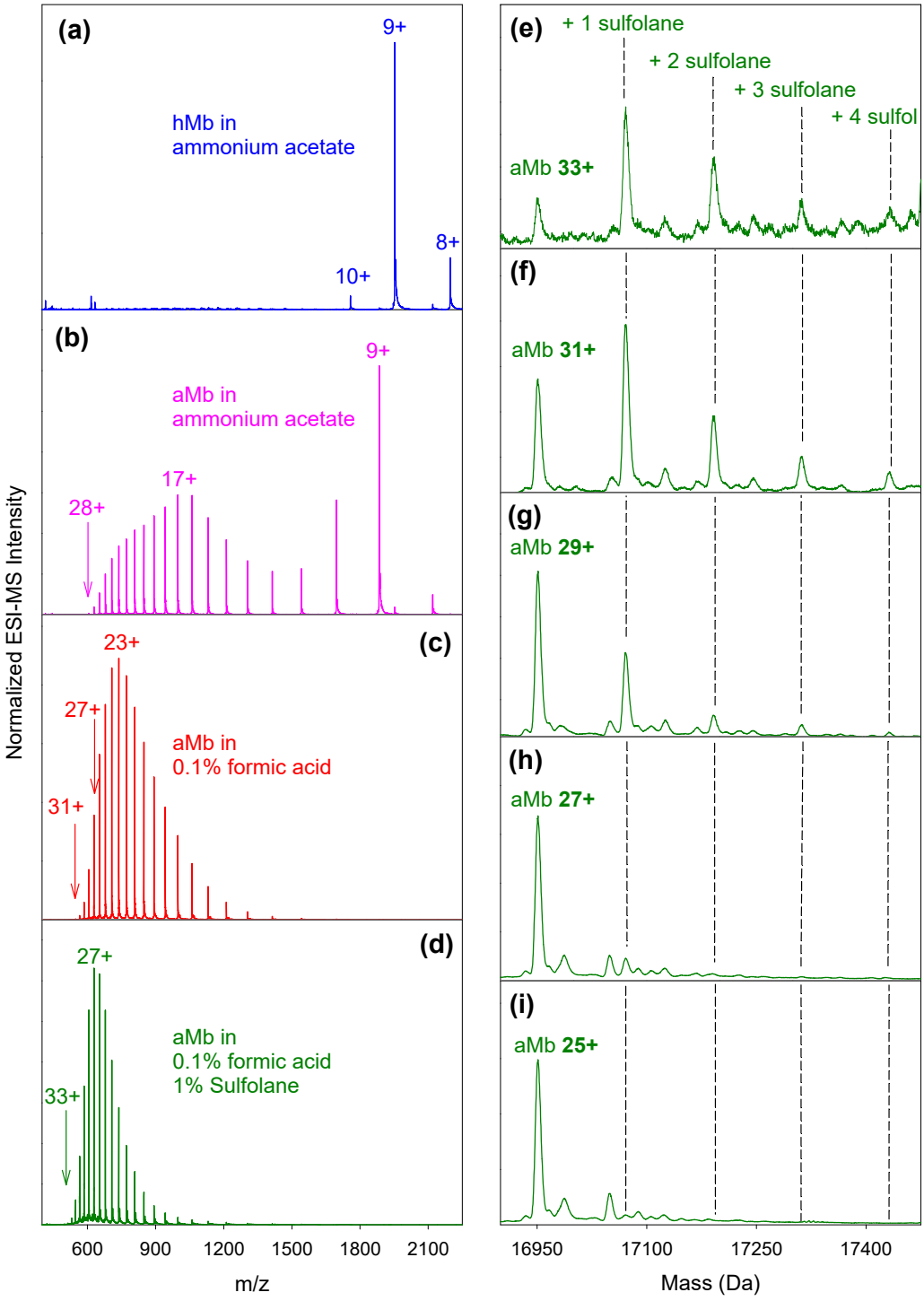
(a)
9+
hMb in
ammonium acetate
8+
10+
(b)
9+
aMb in
ammonium acetate
17+
28+
(c)
23+
27+
aMb in
0.1% formic acid
31+
(d)
27+
aMb in
0.1% formic acid
1% Sulfolane
33+
Normalized ESI-MS Intensity
600
900
1200
1500
1800
2100
m/z
(e)
+ 1 sulfolane
+ 2 sulfolane
+ 3 sulfolane
+ 4 sulfol
aMb 33+
(f)
aMb 31+
(g)
aMb 29+
(h)
aMb 27+
(i)
aMb 25+
16950
17100
17250
17400
Mass (Da)

Figure 3

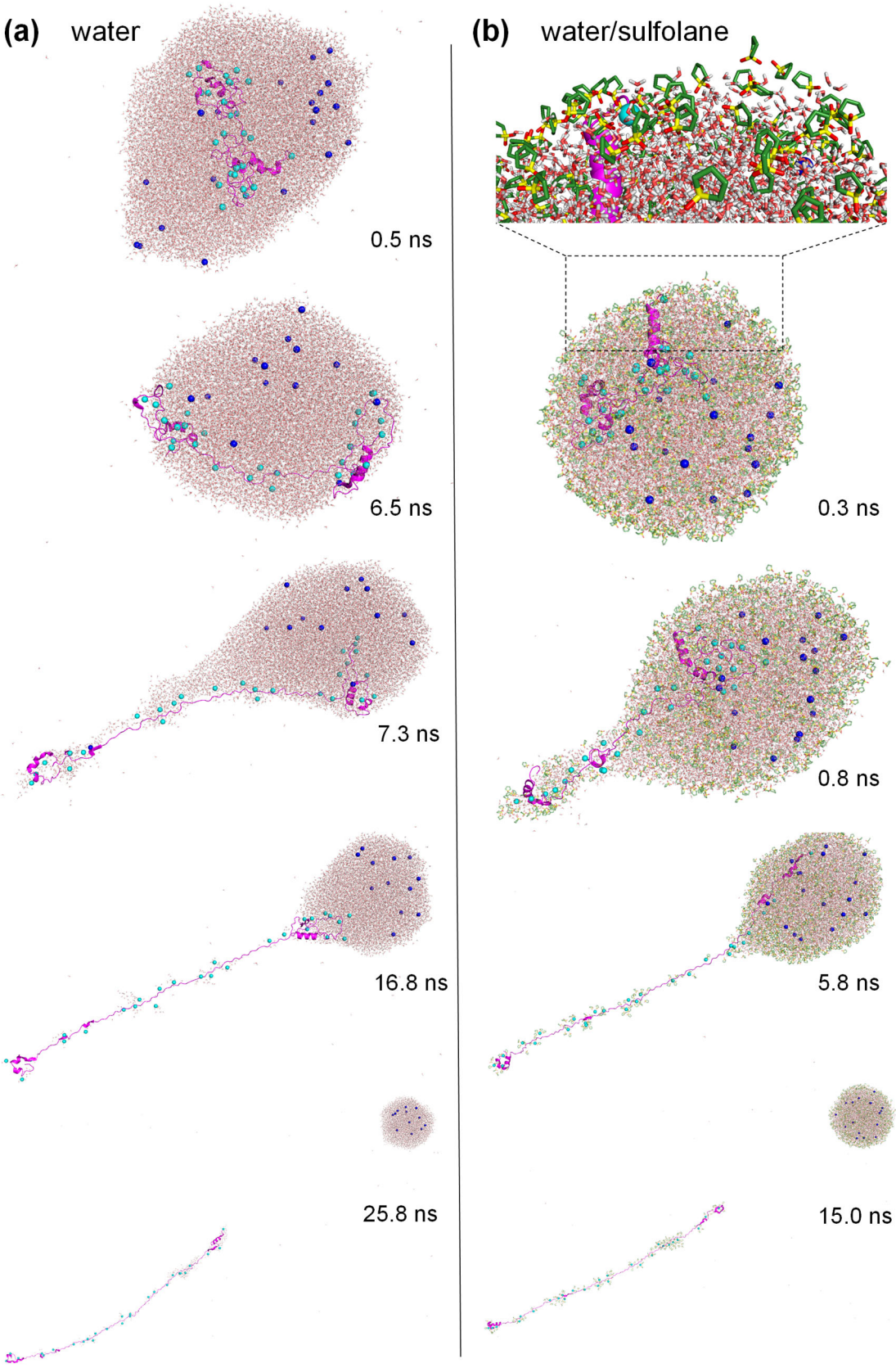
(a) water
0.5 ns
6.5 ns
7.3 ns
16.8 ns
25.8 ns
(b) water/sulfolane
0.3 ns
0.8 ns
5.8 ns
15.0 ns

Figure 4

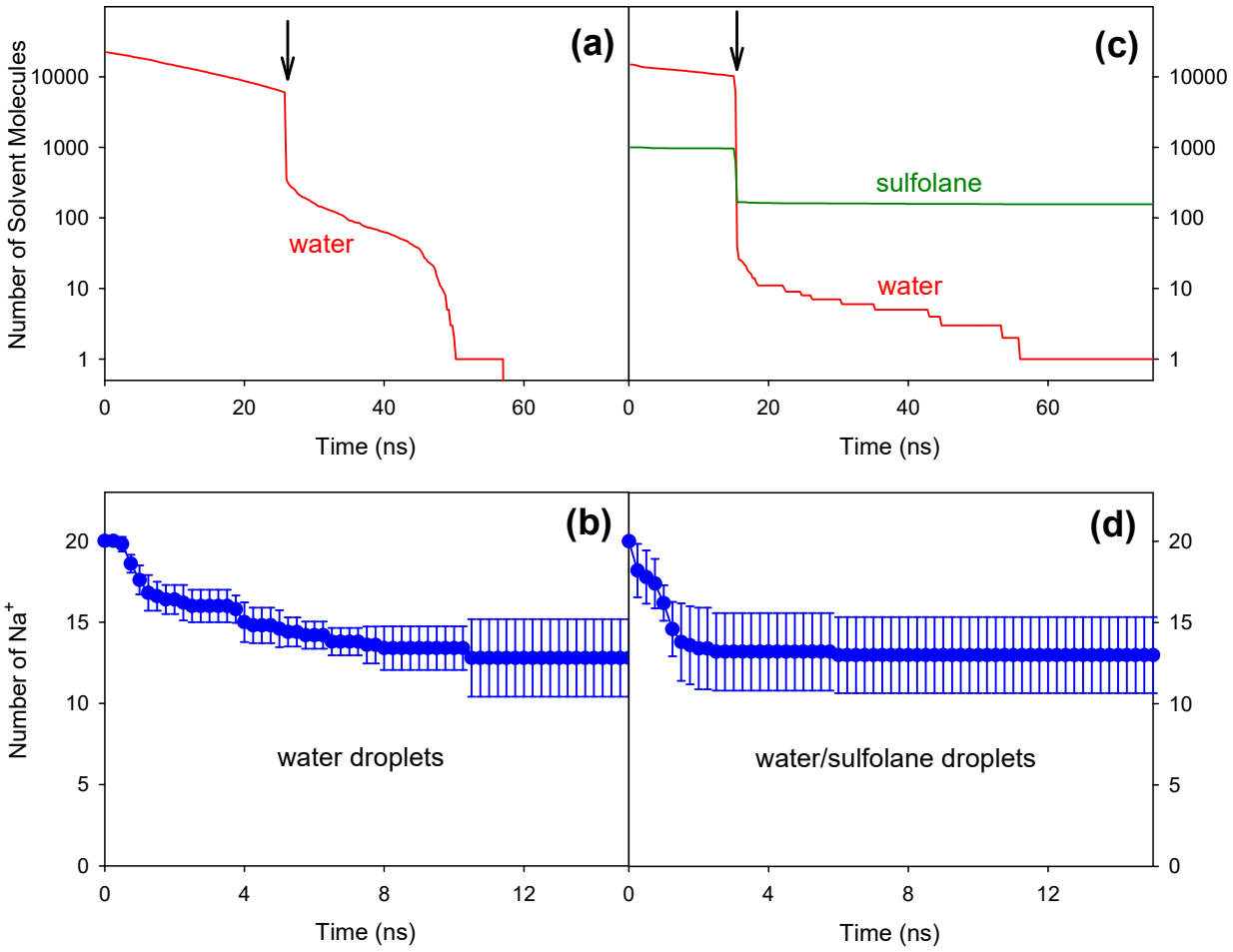
(a)
(c)
(b)
(d)
Number of Solvent Molecules
Number of Na+
Time (ns)
water
sulfolane
water droplets
water/sulfolane droplets
10000
1000
100
10
1
20
15
10
5
0
0
20
40
60
4
8
12

Figure 5

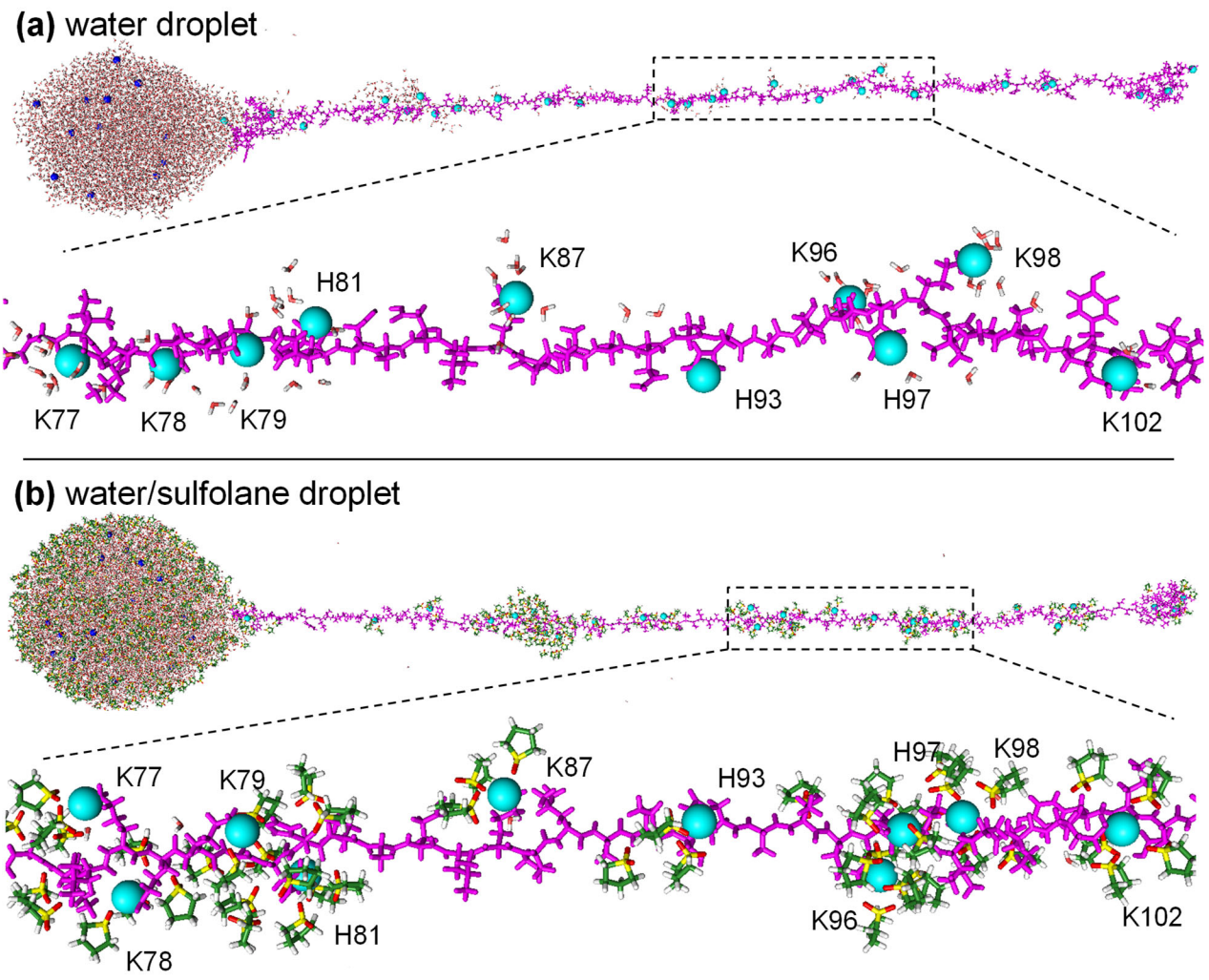
(a) water droplet
K77
K78
K79
H81
K87
H93
K96
H97
K98
K102
(b) water/sulfolane droplet
K77
K79
K78
H81
K87
H93
H97
K98
K96
K102
(c)
water droplet
water/sulfolane droplet
water
water
sulfolane
Number of Solvent Molecules
0
100
200
300
400
500
600
(d)
water droplet
water/sulfolane droplet
E(protein)
E(solvent)
E(total)
Energy of Pos. Charged Residues (kJ mol-1)
5000
2500
0
-2500
-5000
-7500
-10000

Figure 6

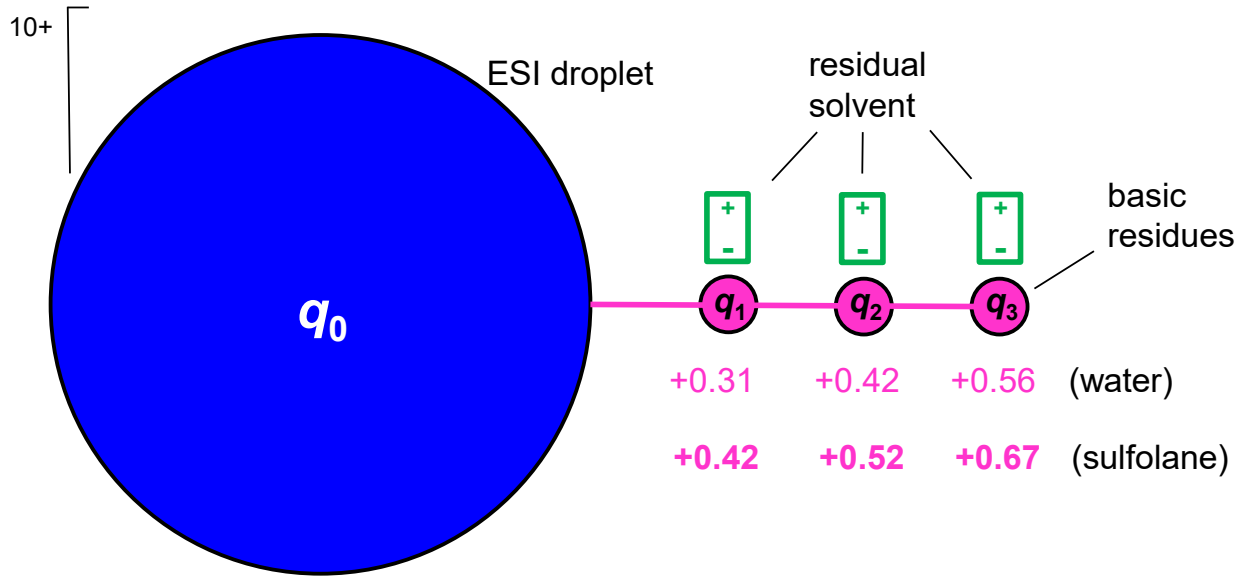
10+
ESI droplet
residual
solvent
basic
residues
q_0
q_1
q_2
q_3
+0.31
+0.42
+0.56
(water)
+0.42
+0.52
+0.67
(sulfolane)

For Table of Contents Only